Corresponding author:
Unai Letamendia;
Email: unai.letamendia@upm.es

Ground-penetrating radar as a tool for determining the interface between temperate and cold ice, and snow depth: a case study for Hurd-Johnsons glaciers, Livingston Island, Antarctica

Unai Letamendia[1] [ID], Francisco Navarro[1] [ID] and Beatriz Benjumea[2] [ID]

[1]Departamento de Matemática Aplicada a las TIC, ETSI de Telecomunicación, Universidad Politécnica de Madrid, Madrid, Spain and [2]Instituto Gelógico y Minero de España, CSIC, Madrid, Spain

Abstract

We analyze the internal structure of two polythermal glaciers, Hurd and Johnsons, located on Livingston Island, Antarctica, using 200 and 750 MHz GPR data collected in 2003/04, 2008/09 and 2016/17 field campaigns. Based on the different permittivities of snow and ice, we determined the thickness distribution of the end-of winter snow cover and of the cold ice layer. Their knowledge is fundamental for mass balance and glacier dynamics studies due to the different densities and rheological properties of such media. The average measured thicknesses for the snow and cold ice layers (the latter including the snow layer) were of 1.44 ± 0.09 and 29.1 ± 1.5 m, and their corresponding maxima were of 2.45 ± 0.21 and 80.8 ± 2.5 m. GPR snow profiling allowed for extension of the coverage of the snow thickness survey, but added little information to that supplied by snow pits, stake readings and manual snow probing, because of the multiplicity of reflections within the seasonal snowpack caused by internal ice layers and lenses. The polythermal structure determined for Hurd Glacier fits into the so-called Scandinavian type, seldom reported for the Antarctic region.

1. Introduction

Knowledge of the internal structure of polythermal glaciers is fundamental to the study of their dynamics. Ground-penetrating radar (GPR) is a suitable tool for determining such structure. This paper focuses on the analysis of the internal structure of two polythermal glaciers located in the Antarctic Peninsula (AP) region. The climate in this region has experienced significant changes over recent decades. During the second half of the 20th century, the AP experienced one of the largest warming trends on the planet, with a rate of $\sim 0.5\,^{\circ}$C per decade at Faraday-Vernadsky station (Turner and others, 2005). Most glaciers in the area retreated over that period (Rau and otherts, 2004; Cook and others, 2016). This warming period was followed, particularly in the northern AP and the South Shetland Islands (SSI), by a brief but sustained cooling period lasting from the late 20th century to the mid-2010s (Turner and others, 2016; Oliva and others, 2017), in turn followed by a return to warming conditions (Carrasco and others, 2021). Climate variations have a direct effect on the hydrothermal structure of glaciers and hence on their dynamic response (Rabus and Echelmeyer, 2002; Pettersson and others, 2007; Gusmeroli and others, 2012). Regional climate also drives surface mass balance (SMB), through both accumulation and ablation processes. Snow accumulation in this region has shown an increasing trend since the 1930s (Medley and Thomas, 2019). Surface melting and runoff, in turn, are fundamentally governed by temperature changes and have therefore followed the above-mentioned temperature trends (Costi and others, 2018).

Hurd and Johnsons are two polythermal glaciers (Navarro and others, 2009; Sugiyama and others, 2019) located on Hurd Peninsula, Livingston Island, which is the second-largest island of the SSI archipelago (Fig. 1). Polythermal glaciers have also been identified at other locations within the SSI, such as King George Island (Wen and others, 1998; Breuer and others, 2006; Blindow and others, 2010). A wealth of glaciological studies are available for these glaciers due to their proximity to the Spanish Antarctic station Juan Carlos I (JCI). These span from mass balance observations (Molina and others, 2007; Navarro and others, 2013) and modeling (Jonsell and others, 2012) to glacier dynamics observations (Machío and others, 2017; Sugiyama and others, 2019) and modeling (e.g. Otero and others, 2010), through other subjects such as geomorphology (Ximenis and others, 2000; Molina, 2014) or front position changes (Rodríguez and Navarro, 2015). Fundamental to our purposes are the local studies focused on radar and seismic applications (Benjumea and others, 2003; Navarro and others, 2005, 2009). A further interest in Hurd and Johnsons glaciers is that their SMB records are part of the World Glacier Monitoring Service (WGMS) database since the hydrological year 2002.

GPR has been widely used for the investigation of glaciers, including their ice-thickness distribution, internal structure (layering, deformation structures), thermal regime, ice properties
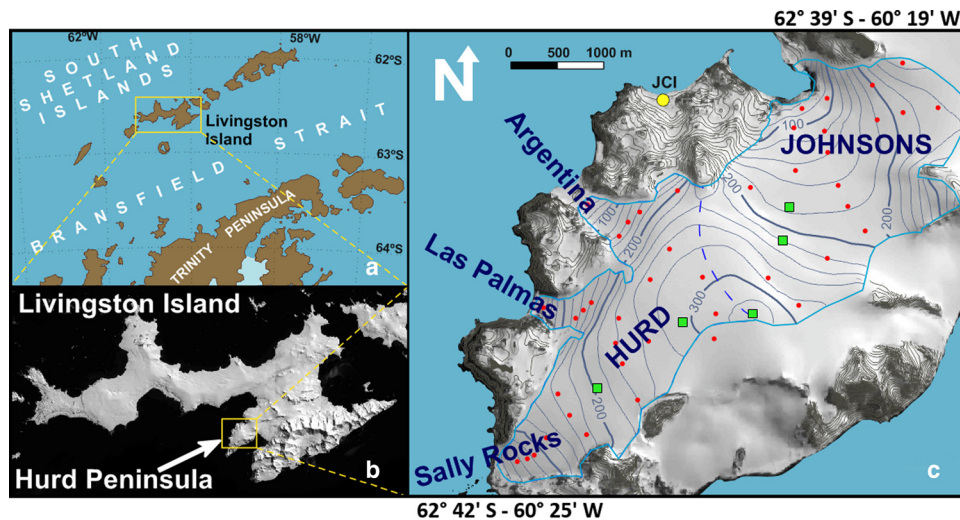
Figure 1. (a) Location of Livingston Island in the South Shetland archipelago. **(b)** Location of Hurd Peninsula on Livingston Island. **(c)** Location and surface elevation of Hurd and Johnsons glaciers. Red dots indicate the location of the mass balance stakes in 2016/17, green squares indicate location of snow pits and the yellow dot indicates the position of Juan Carlos I Station (JCI). The dashed blue line shows the ice divide separating both glaciers. Image modified from Recio-Blitz and others (2018). The Lat./Long. range is indicated in panel c.

(density, water content) and ice-bedrock interface characteristics (presence of water, bed roughness), among others (Schroeder and others, 2020). In the case of polythermal glaciers, knowledge of the internal distribution of cold and temperate ice layers is critical for thermo-mechanical modeling because of the distinct rheological properties of both types of ice (Greve and Blatter, 2009). Such distribution is defined by the so-called cold-temperate transition surface (CTS). Multiple studies have demonstrated the potential for detecting thermal regimes within glaciers through radar surveys (e.g. Eisen and others, 2009; Gusmeroli, 2010; Schannwell and others, 2014). Although several studies on the numerical modeling of Johnsons and Hurd glaciers have been carried out (Martín and others, 2004; Otero and others, 2010; Molina, 2014), all of them consider the glacier as an isothermal ice mass. Having available the current spatial distribution of cold and temperate ice layers would allow a full thermo-mechanical modeling of the evolution of these glaciers using models such as those by Greve (1997); Aschwanden and others (2012).

GPR is also a useful tool for determining the thickness of the snow layer. Such data, when referred to the end-of-winter layer, are essential for accurately estimating the accumulation component of the SMB (e.g. Sold and others, 2013). GPR allows snow thickness measurements to be made much faster than conventional methods (snow probing, snow pits, shallow cores), which are usually very time-consuming (e.g. Harper and Bradford, 2003; Grabiec and others, 2011; McGrath and others, 2018; Laska and others, 2019).

The above considerations motivate the dual focus of this paper, consisting of determining: (1) the thickness distribution of the cold ice layer of Hurd Glacier; and (2) the spatial distribution of the end-of-winter snow depth of Hurd and Johnsons glaciers. This will be achieved through the use of very high and ultra high frequency (VHF and UHF, 200 and 750 MHz respectively, in our case) GPR data collected during the 2003, 2008 and 2016 field campaigns.

2. Geographical setting

Our study area is Hurd Peninsula (62° 39–42'S, 60° 19–25'W; Fig. 1), Livingston Island, SSI, Antarctica. It is covered by an ice cap with an area of ~13.5 km^2 and spans an altitude range

from sea level to ~370 m a.s.l. This ice cap consists of two main basins, Hurd and Johnsons glaciers, plus two additional, smaller basins draining to the southeast that have seldom been studied because they are heavily-crevassed icefalls. Hurd Glacier (4.03 km^2) is a land-terminating glacier, with three main lobes: Argentina, flowing northwestwards, Las Palmas, flowing westwards and Sally Rocks, flowing southwestwards. The later has an average surface slope of about 3°, while Argentina and Las Palmas tongues are much steeper, around 13°. Hurd Glacier is located between 250 and 330 m a.s.l. Hurd Peninsula ice cap has three additional tongues flowing eastwards. These tongues are highly crevassed, preventing in situ field measurements. Johnsons (5.36 km^2) is a tidewater glacier, flowing northwestwards, that terminates at a calving front 50 m in height extending 570 m along the coast. Just a few meters are submerged. Johnsons Glacier typically has surface slopes between 6° and 10°.

Both Hurd and Johnsons glaciers have a polythermal structure showing an upper layer of cold ice, several tens of meters thick in the ablation zone. In the various lobes of Hurd Glacier, the ice thickness gradually decreases to zero at the front, and the cold ice layer reaches the bedrock (Navarro and others, 2009).

The average ice thickness in 1999–2001 of the Hurd-Johnsons ensemble, determined from GPR data, was 93.6 ± 2.5 m (Navarro and others, 2009). Maximum thickness values of Hurd Glacier are ~200 m in the accumulation zone, while those of Johnsons Glacier reach ~160 m. The ice surface velocity of Johnsons Glacier increases towards the ice front, attaining values up to 65 m a^{-1} (Otero and others, 2010; Machío and others, 2017). The highest ice velocities for Hurd Glacier are just about 5 m a^{-1} at its central basin, decreasing towards the frozen-to-bed terminal zones (Machío and others, 2017).

The ice cap on the Hurd Peninsula is exposed to the maritime weather of the western AP. The warmest temperatures in Antarctica have been recorded in the AP (Francelino and others, 2021). The annual average temperature at JCI station during the period 1994–2014 was −1.2 °C, with average summer and winter temperatures of 1.9 °C and −4.7 °C (Bañón and Vasallo, 2016). On Hurd and Johnsons glaciers, the mass gain is mostly by snowfall and wind-driven snow redistribution (Navarro and others, 2013). The predominant winds on Hurd Peninsula, measured at Johnsons Glacier automatic weather station, are from the north-northeast and the southwest (Fig. 2). Since 2002, the seasonal
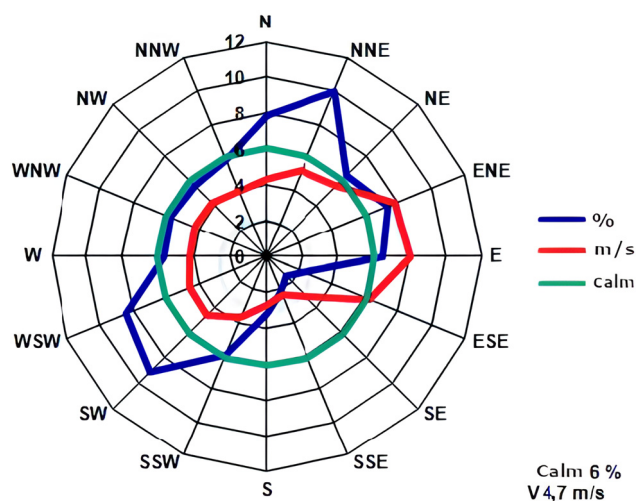
Figure 2. Wind-rose graph of Johnsons Glacier automatic weather station for the period December 2006-December 2014. Image modified from Bañón and Vasallo (2016).

and annual SMB of both glaciers have been measured using the glaciological method, with average values over the period 2002–2021 very close to zero (Zemp and others, 2021).

3. Field data and processing

For this work we used data from the austral summer campaigns 2003/04, 2008/09 and 2016/17, collected using different radar systems as detailed in Table 1. The higher vertical resolution of the 750 MHz radar is suitable for the analysis of the shallowest structures, namely the snow cover. The VHF 200 MHz radar, in turn, provides greater penetration, at the expense of a lower resolution, and allows analysis of deeper structures, such as the CTS. Common offset profiling was carried out in all cases. In the 2003 and 2016 campaigns, the radar equipment was installed on a sledge towed by a snowmobile. In 2008 campaign it was towed by a skier. Radar trace positioning was achieved by means of GNSS measurements. In the 2003 and 2008 campaigns, single-frequency GNSS was used, implying a horizontal positioning accuracy of ∼3 m, but occasionally up to ∼5 m. Differential GNSS measurements (centimetric accuracy) at each profile endpoints served as an additional control of the positioning (GPR profiles are carried out at nearly-uniform speed). In these campaigns, the positioning by single-frequency GNSS often provided non-reliable coordinates for the profiles (e.g. radar profiles in a zigzag), so we opted for assigning to the traces coordinates based on the accurately-positioned endpoints and the assumption of a regular traction speed. In the 2016 campaign, differential GNSS was used, involving centimetric accuracy for the positioning. The GNSS-measured coordinates were directly inputted to the GPR recording unit.

In all three campaigns, fieldwork also included snow probing (i.e. measuring the snow depth using an avalanche probe) in the network of ca. 50 mass balance stakes deployed on both glaciers plus 50 other locations, making a total of about 100 measurements. These data were used primarily for the snow depth map but are also useful to determine the thickness of each layer in the cases of the snow-firn column and snow-cold ice column, for the accumulation and ablation zones, respectively. These measurements were complemented by snow pits at 5 locations (Fig. 1). The snow pits were measured twice per campaign, close to the beginning and to the end of the summer season. This allows estimation of the changes in density of the snowpack (including internal ice layers and lenses) during the melting season.

Radar data processing was similar in all cases. The time-zero was adjusted according to the timing of the first arrivals. The DC offset was corrected using a bandpass filter, with cutoff frequencies 0.5 and 1.5 times that of the central frequency. To reduce the disturbing effects from the air and ground (snow/ice surface) direct waves, as well as the antenna ringing effects, we used background removal. Amplitude scaling was applied to remove attenuation effects with depth. Migration was used to move the position of the reflectors to their true positions and to collapse the diffractors, increasing the spatial resolution.

4. Methods

The time-to-depth conversion was done using

$$H = \frac{1}{2}v\tau, \tag{1}$$

where v is the radar wave velocity (RWV) and τ is the two-way travel time from the transmitter to the reflector and back to the antennas, which is the field-recorded quantity. From the thickness measurements, corresponding maps were created using Surfer software and ordinary kriging interpolation.

4.1 Seasonal snow depth

The 2016 end-of-winter snow cover of Hurd and Johnsons glaciers was obtained by combining GPR-derived snow thickness and snow probing data. Note that, in snow studies, snow depth denotes the total height of the snowpack measured in the vertical direction, while the thickness of the snowpack is measured perpendicular to the surface slope (Fierz and others, 2009). If the surface slope is small, both quantities are close to each other. When using GPR to measure the snowpack things become more complex. The wave path of the signal received upon reflection at the bed is not dictated by the perpendicular to the surface but by the perpendicular to the bed at the reflecting point. Therefore, if snow surface and snow bed are not parallel, this introduces distortions in the radar signals that could be corrected through procedures such as migration and topographic correction. Fortunately, in most cases snow surface and base are nearly parallel and, under such conditions, what we get from the GPR measurements is the thickness (not depth) of the snowpack. In our case study, the surface slopes are gentle, and therefore snow depth and snow thickness are very similar, which justifies combining measurements from snow probing and GPR data.

Table 1. Radar surveys carried out on Hurd Peninsula, radar systems used and total profiles length

Campaign	Glacier	Radar (frequency)	Antenna layout	Antenna separation	Triggering	No. of profiles	Distance covered
Dec. 2003	Hurd & Johnsons	Måla GS Ramac/ GPR (200 MHz)	Broadside/ End fire	0.6 m 1 m	Odometer (0.2 m)	88	72 km
Dec. 2008	Hurd	Måla GS Ramac/ GPR (200 MHz)	End fire	0.6 m	Odometer (0.25 m)	15	5.6 km
Dec. 2016	Hurd & Johnsons	Måla GS GX750 (750 MHz)	–	0.14 m	Time (0.1 s)	44	30.5 km

Each trace of the GX750 GPR spans 274 ns, discretized into 2636 samples taken every 0.1 ns. This time window is sufficient to sample the whole column of the seasonal snow cover.

The depth-averaged RWV in snow was determined from the two-way travel time at 48 points in the radar profiles close to the locations of the snow-thickness measurements by snow probing. This RWV was used for the conversion from two-way travel time to snow thickness at all radar profiles.

A fundamental problem for the determination of the end-of-winter snow depth, no matter whether from GPR or snow probing data, is the presence of multiple internal ice layers and lenses within the end-of-winter snowpack. A sample radargram illustrating these difficulties is shown in Fig. 3. The availability of ca. 50 accumulation/ablation stakes across Hurd and Johnsons glaciers allows us to determine a lower bound of the end-of-winter snow depth. This bound is simply obtained as the difference between the stake readings at the end-of-winter and at the end of the previous summer. Actually, this difference is in itself the definition of the winter accumulation layer thickness. The reason for considering it as a lower bound is that Juan Carlos I station is operated only during the austral summer. The last measurements in the campaign are therefore done before station closing, which usually takes places a couple of weeks before the actual end of the summer melting. Snow probing is also made next to these 50 stakes, allowing us to validate the additional 50 snow probe measurements done at locations different from those of the stakes. Further validation data is provided by the 5 snow pits mentioned in the Field data and processing section. Summarising, snow pits, stake readings and snow probing data help in identifying the snow-firn/ice interface from the GPR data.

4.2 Cold ice layer thickness

The cold ice layer of Hurd Glacier was analyzed using profiles taken in the 2003/04 and 2008/09 campaigns. All of the profiles collected in the 2008/09 campaign were used, whereas, for the 2003/04 campaign, only those profiles for the ablation zone of Hurd Glacier were employed (14 out of the 88 shown in Table 1). Since its thickness was measured from GPR profiling at the glacier surface, it actually includes the thickness of the thin overlying seasonal snow cover (~1.2 m on average for the 2008/09 campaign). In certain areas, the time window used for the 2003/04 profiles (~430 ns) was insufficient to detect the CTS. This problem is absent in the 2008/09 data, in which a time window of ~1100–1500 ns with a sampling period of 1 ns

was used. For the RWV of cold ice a standard value of 168 m μs^{-1} was used (Macheret and others, 1993). Note that the cold ice layer is only present in the ablation zone. Therefore, we are just neglecting the higher RWV velocity of a thin (1–2 m) snow layer. Consequently, only the zones with a very thin cold ice layer will be affected by our assumption of a constant RWV. The CTS was manually determined as the transition between the clean, upper part of the radargram devoid of internal reflections/diffractions (cold ice), and the lower part with plenty of diffractions caused by the liquid water in temperate ice (Fig. 4).

4.3 Error estimation

The uncertainty in depth of the GPR measurements was derived from equation (1) using error propagation:

$$e_{H_m} = \frac{1}{2} \left(\tau^2 e_v^2 + v^2 e_\tau^2 \right)^{1/2}. \tag{2}$$

e denotes the error in the variable indicated by the corresponding subscript.

The error in RWV for the seasonal snow cover was taken as the standard deviation mentioned earlier. This error was found to be within the vertical resolution of the instrument, which is theoretically $\lambda/4$, with λ the wavelength, but can in practice reach up to $\lambda/2$ (Navarro and Eisen, 2009). To construct the snow-depth map (Fig. 5), point values were spatially interpolated using kriging. Due to the abundance of quite homogeneously distributed measurement points, we took the interpolation error as the standard deviation of the leave-one-out cross-validation (a single value for the whole glacier).

In the case of cold ice, the error in RWV was taken from Navarro and others (2009). Measurement errors for the cold ice thickness higher than the vertical resolution were obtained in zones of deep ice, reaching values up to 1 m. The determination of the CTS involves interpretation errors due to the diffuse boundary between the cold and temperate ice layers. We estimated this interpretation error following the technique described in Gusmeroli (2010), whereby 25 sets of pickings of the CTS were performed by three different researchers. The CTS point value was taken as the average of the 25 picks (shown as red line in Fig. 4), and its standard deviation (blue-shadowed band in Fig. 4) was assigned as error e_{H_p}. Measurement and interpretation errors were combined as

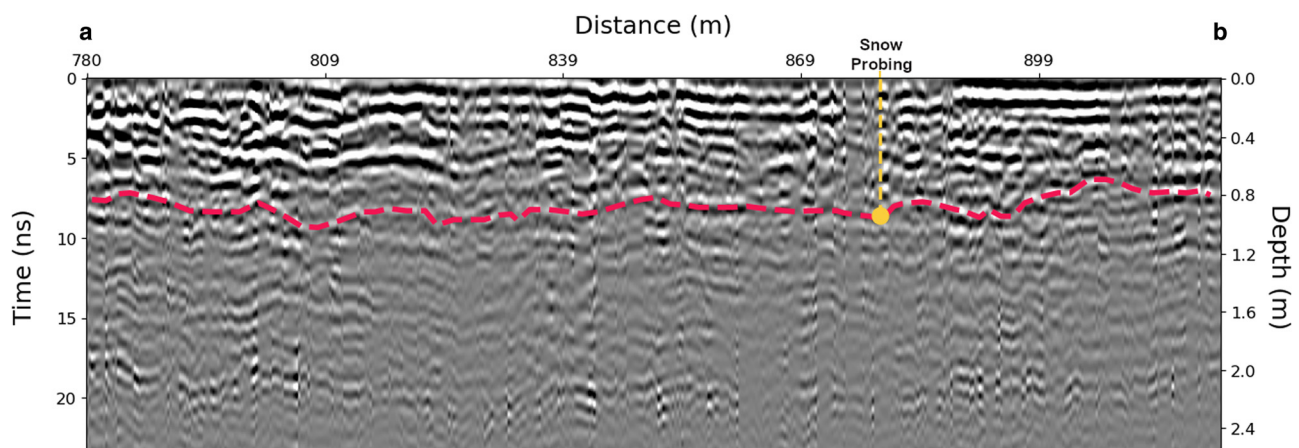$$e_{H_d} = \sqrt{e_{H_m}^2 + e_{H_p}^2}. \tag{3}$$

Figure 3. Radargram of a 750 MHz GPR profile registered on Hurd Glacier in December 2016 . The red dashed line indicates the end-of-winter snow depth. The yellow dot marks the depth of the snow layer determined by snow probing. The location of this profile is shown by the red segment in Fig. 5a (A to B).
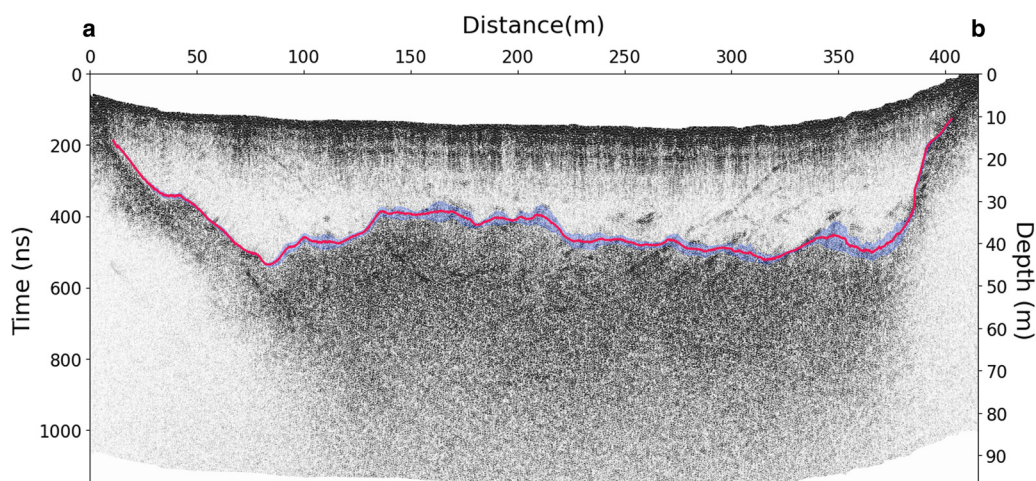
Figure 4. Topographically-corrected radargram of GPR 200 MHz profile registered on Hurd Glacier in December 2008, with the CTS outlined in red and its interpretation error as a blue band; cold ice in contact with bedrock is also shown in red. The location of this profile is shown by the red A-B segment in Fig. 8a. The time and depth scales are assumed to start from the beginning of each trace.

The construction of the cold ice thickness map was also based on a kriging interpolation. However, as the source data comes from GPR profiling, there is a high data density along the radar profiles, while there exist large data gaps between the profiles. Therefore, we followed the procedure for computing the interpolation error, and combining it with e_{H_d}, described by Lapazaran and others (2016).

5. Results and discussion

5.1 Seasonal snow depth

The mean of the depth-averaged RWV in snow determined at 48 points (see Methods section) was $v = 210.0$ m μs^{-1}, with a standard deviation $\sigma = 5.3$ m μs^{-1}, which is within the expected range of values for such media (e.g. Moore and others, 1999). This velocity value is typical of dry snow. This is consistent with the fact that our measurements were done before the onset of summer melting. The presence of thin internal ice layers and lenses within the snowpack reveals that some surface melting with subsequent meltwater percolation and refreezing happened, likely in high-temperature peaks during the late spring. However, the winter snowpack was mostly dry when the end-of-winter snow pits were measured, which justifies the mentioned velocity typical of dry snow. Furthermore, Recio-Blitz and others (2018) reported a mean end-of-winter density of 510 ± 14 kg m^{-3} at Hurd and Johnsons glaciers over the period 2004–2016. If we use this value with Robin's equation $\varepsilon = (1 + 0.851\rho)^2$ (Robin and others, 1969), relating density ρ and permittivity ε of dry snow, and then apply the relationship $v = c/\sqrt{\varepsilon}$ (Dowdeswell and Evans, 2004), with c the radar wave velocities in free space, we get a radar wave velocity in snow of 209.2 ± 1.8 m μs^{-1}.

The 2016 seasonal snow depth maps, based on manual snow probing and snow probing combined with GPR are shown in Figures 5(a,b) respectively. The average snow depth from snow probing measurements was 1.44 m ± 0.09 m (the quoted error is the standard deviation). The largest values were found in the higher-elevation areas of the glaciers. The maximum snow depth, of 2.45 ± 0.21 m, was found in the northern part of Johnsons Glacier, where snow redistribution by wind accumulates a large amount of snow (see Fig. 2) . The interpolation error associated with the snow depth map is 0.42 m.

The distribution of snow accumulation on both glaciers depends on both meteorological and orographic conditions. The altitude range of these glaciers is in the order of 300 m, so there is a moderate difference between the amount of snow initially deposited at high and low altitudes. The linear fit of snow depth vs elevation shown in Fig. 6 spans a range of ~1 m. However, the glacier
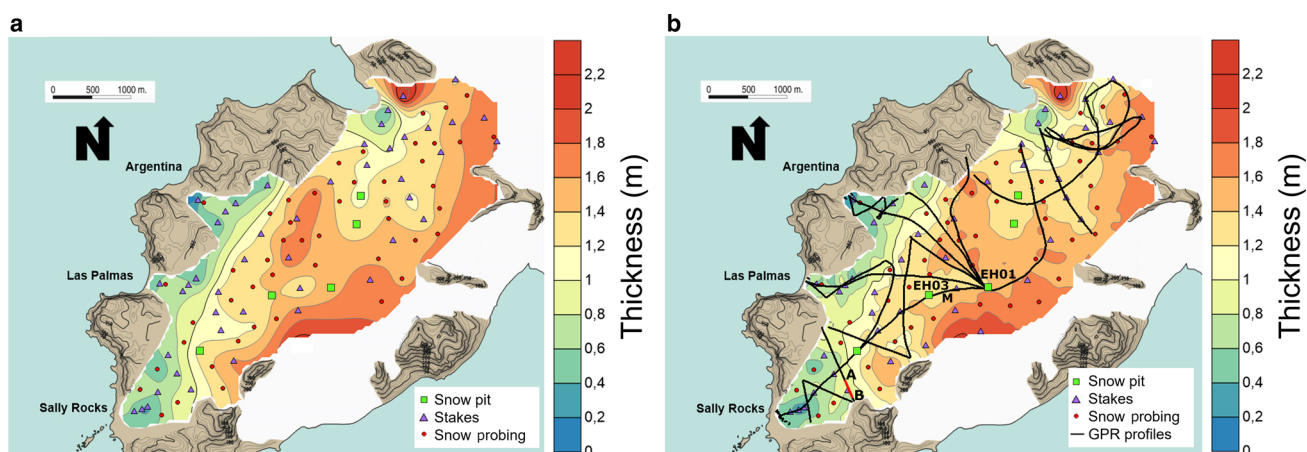

Figure 5. (a) End-of-winter snow depth map for December 2016 based on stake and snow probe measurements. (b) Same as (a) but adding the thickness obtained from GPR snow layer profiling. The red segment A to B is the location of the profile shown in Fig. 3.
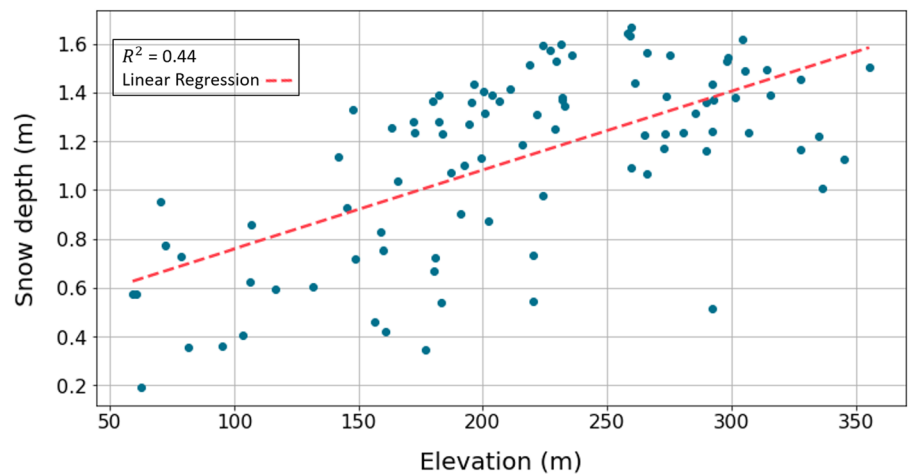
Figure 6. Combined end-of-winter snow depth for Hurd and Johnsons glaciers in December 2016 and linear fit to the data.

hypsometry implies that most of the glacier area is concentrated in a relatively narrow altitude range (150–300 m), and therefore most data points are clustered in the mentioned elevation range, for which the snow depths vary between 1.0 and 1.6 m. Consequently, the variation of snow depth with elevation is not a critical issue. On the other hand, snow redistribution by the prevailing north-north-easterly and south-westerly winds (Fig. 2) causes slightly higher accumulations on Johnsons Glacier, and in general in the concave parts of both glaciers. In particular, the south-westerly winds remove by erosion part of the snow initially deposited on the upper reaches of Hurd glacier and deposit it on the more concave Johnsons Glacier. This results in systematically more positive winter (and annual) surface mass balances in Johnsons Glacier as compared with Hurd Glacier (Navarro and others, 2013). On the other hand, higher temperatures at lower elevations imply a higher degree of compaction of the snow, and hence a thinner snow layer. Compaction alone, however, is insufficient to explain the difference in snow depth between the upper and lower elevations. Some additional factors have to be taken into account. Rain should in principle be discarded, as it normally occurs much later in the season. However, some surface melting and runoff at the lowermost part of the ablation zone should not be discarded; another intervening process could be the erosion of snow away from the glacier at the lowermost elevations. Unfortunately, for most of these processes, we lack observational evidence, so we cannot quantify their influence.

The data recorded with the GX750 in 2016 present a large amount of noise and stratification, mostly due to refreezing of percolating surface meltwater. Although the field measurements were carried out in the early austral summer, before the onset of strong surface melting, some melting and subsequent percolation and refreezing of meltwater happen in the glaciers in this region during the late spring (Recio-Blitz and others, 2018). The wavelength (λ) of our 750 MHz radar in snow (RWV = 210 m μs^{-1}) is 0.28 m, so its vertical resolution is between 0.07 m ($\lambda/4$) and 0.14 m ($\lambda/2$). Ice layers and lenses observed in the snow pits are in general thinner than this (typically ca. 1–3 cm). However, the radar wave actually integrates the energy reflected from all discontinuities in physical properties within a spatial range equal to its resolution. At the glaciers under study, quite often adjacent thin ice layers are separated by distances lower than the radar resolution and can therefore be detected, though not resolved individually. Also thin individual layers will be detectable when they have strongly altered electrical properties. However, this is not the usual case in glacier environments. Because of such noise, the interpretation of the seasonal snow layer would not have been possible without the additional information provided by the data analysis of stake readings, snow probing, and snow pit measurements. In fact, in our case study it was often impossible to track the GPR internal layers (in particular, the snow–ice and snow–firn transition surfaces) between manual point measurements (snow pits, stake readings, snow probing). This is illustrated in Fig. 7, where we can see
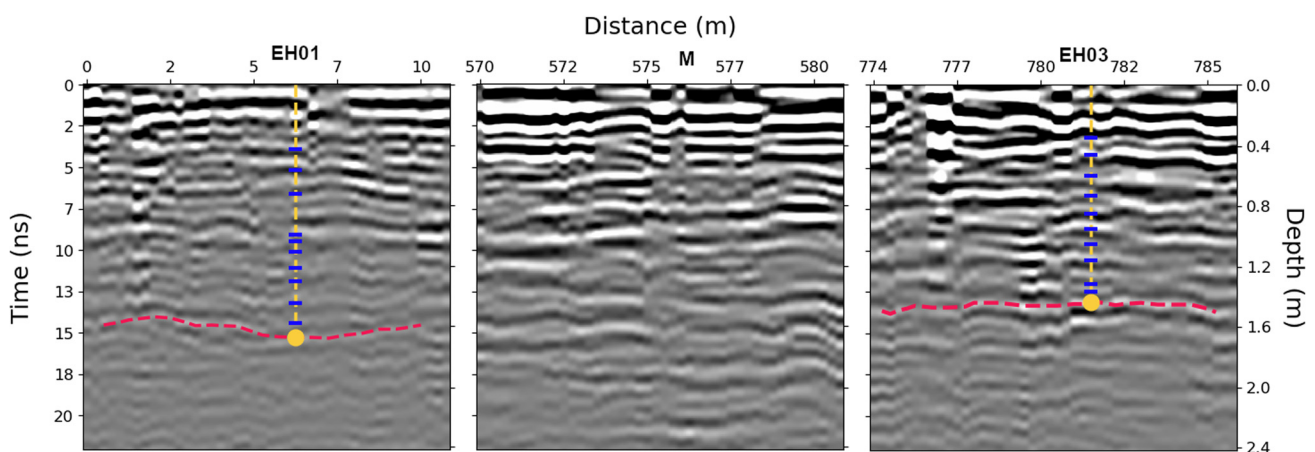

Figure 7. Sections of a radargram of a 750 MHz GPR profile registered in December 2016. The radargrams at both sides correspond to locations adjacent to snow pits EH01 and EH03, while the central one (marked M) corresponds to a location in between both boreholes. Their locations are shown in Fig. 5b. The red dashed line indicates the end-of-winter snow depth. The yellow dot marks the depth of the snow layer determined at the snow pits. The blue lines indicate the location of refreezing layers measured in the snow pits.
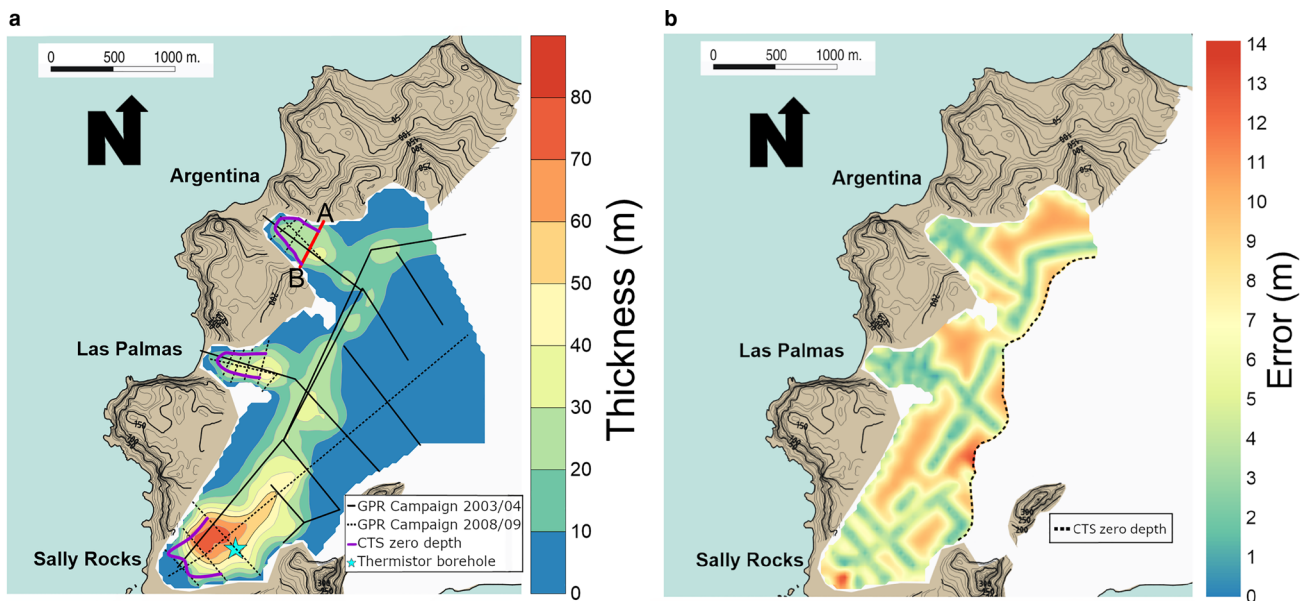
Figure 8. (a) Cold ice-thickness map retrieved from the radar measurements. The red segment A–B indicates the radar profile shown in Fig. 4. (b) Spatial distribution of the total error in thickness of the cold ice layer.

that, although close to the snow pits, the snow–firn interface can be identified with the help of the snow depth determined at the pit, but when we move away from the pit such an interface cannot be longer tracked. The central panel of Fig. 7 shows a section of a radargram at an intermediate distance between two snow pits, and we are unable to identify which is the layer corresponding to the snow–firn interface. In fact, the distribution of layers and lenses of refrozen ice has a high spatial variability even at short-scale distances. Note that there is often no correspondence between the ice layer location determined in the snow pits (shown as blue lines in the two lateral panels of Fig. 7) and the occurrence of internal reflections in radargrams taken just 5–10 m from the snow pits. Consequently, the snow-thickness product that includes the GPR data does not improve significantly on previous observations from stake measurements such as that by Navarro and others (2013). This contrasts with other studies in which high-frequency radar profiling added important information (Harper and Bradford, 2003), or even constituted the main source of data, with snow pits/probing providing calibration and validation data (Grabiec and others, 2011).

Calibrating the snow layer thickness identified in the radargrams with snow depth from the probing measurements could result in small differences between the snow depth maps shown in Figures 5a,b. The map incorporating the GPR data (Fig. 5b) provides additional detail due to greater data coverage.

5.2 Cold ice layer thickness

The polythermal structure of Hurd Glacier, first suggested by Navarro and others (2009), can be inferred from Fig. 8a, which shows the thickness of the cold ice layer, while Fig. 8b shows the error in thickness. The cold ice layer is only present at lower elevations, basically corresponding to the ablation zone. Its average thickness is 29.1 ± 1.5 m (this error is the mean of the individual measurement errors), and the highest values are found along the central flowline in the lower ablation zone of Sally Rocks tongue, where the thickness of the cold layer reaches its maximum value of 80.8 ± 2.5 m. The ice below the firn layer in the accumulation zone is temperate, and the thickness of the corresponding layer gradually decreases towards the glacier snouts in all lobes of Hurd Glacier. The ice in the frontal zones is cold,

meaning that the glacier is frozen to bed. The purple lines in Fig. 8a indicate where the CTS reaches zero value, meaning that the glacier is frozen to bed from those lines to the glacier margins. This distribution of the cold and temperate ice layers is characteristic of so-called Scandinavian type glaciers, typical of the Scandinavian and Svalbard regions (Aschwanden and others, 2012), but seldom reported in sub-Antarctic islands such as the South Shetland Islands. In this archipelago, in addition to our studied glaciers in Livingston Island, polythermal glaciers have been reported or suggested in King George Island, either from borehole temperature data (Wen and others, 1998), from modeling studies (Breuer and others, 2006), or from GPR data (Blindow and others, 2010). Other glaciers and ice caps in this archipelago with a similar morphology, particularly those ending on land, could be expected to be polythermmal. Having the ice frozen to bed in the terminal zone of a land-terminating glacier has strong implications for glacier dynamics. The largest velocities found in the central part of the glacier sharply decrease when approaching the terminus, resulting in strong compression, often accompanied by reverse faulting (Molina and others, 2007).

The errors in cold ice layer thickness shown in Fig. 8b, calculated combining the method by Lapazaran and others (2016) and the interpretation error, are lower along the locations of the radar profiles, as a consequence of the interpolation error, except in the middle part of the central flow line, where the maximum CTS interpretation error occurred. The dashed line in the figure indicates the zero depth of the CTS, which approximately corresponds to the location of the equilibrium line. As the ice below the firn is temperate, the cold ice layer thickness is zero to the east of the dashed line. Consequently, the errors in cold ice thickness in that zone are meaningless and we have blanked them.

The largest values of the cold layer thickness of Hurd Glacier have been confirmed by thermistor chain measurements in boreholes. In Fig. 8 we have indicated the location of a borehole drilled in January 2015, where a string of 32 thermistors, spaced 2 m apart, was installed. They were first measured one year later, to ensure that the thermistor temperatures were in equilibrium with the neighboring ice. All temperatures were below 0 °C. Unfortunately, the CTS depth was larger than expected for this zone, so the lowermost thermistor, at a depth of 60.55 m below the ice surface, did not reach melting temperature; it measured

∼−0.15 °C. Taking into account the readings of the above thermistors, the CTS could be located at a depth between 60 and 70 m. This CTS depth is larger than that measured in a borehole drilled in Johnsons Glacier in January 2015, where a CTS depth lower than ∼50 m was found (at another borehole, closer to the glacier calving front, only temperate ice was identified) (Sugiyama and others, 2019).

The temperature of the cold ice measured at 15 m depth at Hurd borehole (located at 116 m a.s.l.) was of −1.1 °C. Corresponding values for ice cores at King George Island recovered in the summer of 1991/92 were −1.9 °C (site at 100 m a.s.l.) and −1.4 °C (site at 150 m a.s.l.) (Wen and others, 1998). For comparison with other regions, these values are similar or slightly warmer than those measured at comparable elevations on Scandinavian-type glaciers in Svalbard, where e.g. 15-m depth temperatures at East Grönfjordbreen, at sites between 160 and 225 m a.s.l., provided values of ∼−2°C (Chernov and others, 2015); at Hansbreen, values were between −1.6 and −1.8 °C at a site at ∼160 m a.s.l., and between −2.4 and −3.1 °C at another site at ∼240 m a.s.l. (Jania and others, 1996). The reason for the slightly lower borehole temperatures in Svalbard is probably that the mean annual air temperatures in Svalbard (e.g. −5.2 °C at Ny-Alesund and −4.6 °C at Svalbard Airport over the period 1981–2010; Førland and others, 2011) are colder than those at the South Shetland Islands (e.g. −2.2 °C at Bellingshausen Station, King George Island, over the period 1986–2015; Oliva and others, 2017). Nevertheless, in both cases the warmer temperatures at 15-m depth as compared with the mean annual temperature probably reflect the importance of meltwater refreezing on the release of latent heat (Jania and others, 1996).

6. Conclusions

From the above discussion, the following conclusions can be drawn:

1. Although GPR has been shown elsewhere to be an efficient tool for determining the end-of-winter snow cover thickness with wide coverage (Harper and Bradford, 2003; Grabiec and others, 2011; McGrath and others, 2018; Laska and others, 2019), in our case study it hardly provided any further information to that given by manual snow probing. The reason was the abundance of internal reflections by multiple snow layers and lenses formed from refreezing of percolating meltwater, which prevented the identification of the snow–ice/firn interface without the help of the snow-probed depths. The set of around one hundred snow probing points alone provided a satisfactory snow depth map.

2. The available data suggest that the distribution of the end-of-winter snow cover of Hurd and Johnsons Glaciers (with average and maximum thicknesses of 1.44 ± 0.09 and 2.45 ± 0.21 m, respectively, in 2016/17) is governed by a combination of snow redistribution by the prevailing winds, the greater compaction rates at lower elevations, the erosion of snow away from the glacier and possibly some surface melting and runoff, the two latter processes at the lowermost part of the ablation zone.

3. The spatial distribution of the cold ice layer thickness of Hurd Glacier (with average and maximum measured values of 29.1 ± 1.5 and 80.8 ± 2.5 m, respectively) reveals a Scandinavian-type polythermal structure. Such a structure has often been reported at other locations (e.g. Scandinavia and Svalbard), but seldom in Antarctica. This polythermal structure has important dynamical and geomorphological implications in terms of compressional regime at the glacier snout and associated reverse faulting. The polythermal structure could be a more common feature of South Shetland Island glaciers and ice caps than suggested by the scarce literature on the matter, in particular for land-terminating ice masses.

Due to the climate evolution of this region (Turner and others, 2016; Oliva and others, 2017), it would be of interest to repeat some of the GPR soundings reported in this paper, in particular those regarding the polythermal structure. This would allow analysis of the evolution of the CTS in response to regional climate changes.

References

Aschwanden A, Bueler E, Khroulev C and Blatter H (2012) An enthalpy formulation for glaciers and ice sheets. *Journal of Glaciology* **58**(209), 441–457. doi: 10.3189/2012JoG11J088

Bañón M and Vasallo F (2016) *AEMET en la Antártida: climatología y meteorología sinóptica en las estaciones meteorológicas españolas en la Antírtida.* Madrid: AEMET.

Benjumea B, Macheret YY, Navarro FJ and Teixidó T (2003) Estimation of water content in a temperate glacier from radar and seismic sounding data. *Annals of Glaciology* **37**, 317–324. doi: 10.3189/172756403781815924

Blindow N and 8 others (2010) Geometry and thermal regime of the King George Island ice cap, Antarctica, from GPR and GPS. *Annals of Glaciology* **51**(55), 103–109. doi: 10.3189/172756410791392691

Breuer B, Lange MA and Blindow N (2006) Sensitivity studies on model modifications to assess the dynamics of a temperate ice cap, such as that on King George Island, Antarctica. *Journal of Glaciology* **52**(177), 235–247. doi: 10.3189/172756506781828683

Carrasco JF, Bozkurt D and Cordero RR (2021) A review of the observed air temperature in the Antarctic Peninsula. Did the warming trend come back after the early 21st hiatus? *Polar Science* **28**, 100653. doi: 10.1016/j.polar.2021.100653

Chernov RA, Vasilyeva TV and Kudikov AV (2015) Temperature regime of upper layer of the glacier East Grönfjordbreen (West Svalbard). *Ice and Snow* **131**(3), 38. doi: 10.15356/2076-6734-2015-3-38-46

Cook AJ and 5 others (2016) Ocean forcing of glacier retreat in the western Antarctic Peninsula. *Science* **353**(6296), 283–286. doi: 10.1126/science.aae0017

Costi J and 7 others (2018) Estimating surface melt and runoff on the Antarctic Peninsula using ERA-Interim reanalysis data. *Antarctic Science* **30**(6), 379–393. doi: 10.1017/S0954102018000391

Dowdeswell JA and Evans S (2004) Investigations of the form and flow of ice sheets and glaciers using radio-echo sounding. *Reports on Progress in Physics* **67**(10), 1821–1861. doi: 10.1088/0034-4885/67/10/R03

Eisen O, Bauder A, Lüthi M, Riesen P and Funk M (2009) Deducing the thermal structure in the tongue of Gornergletscher, Switzerland, from radar surveys and borehole measurements. *Annals of Glaciology* **50**(51), 63–70. doi: 10.3189/172756409789097612

Fierz C and 8 others (2009) *The International Classification for Seasonal Snow on the Ground.* IHP-VII Technical Documents in Hydrology N°83, IACS Contribution N°1, UNESCO-IHP, Paris.

Førland EJ, Benestad R, Hanssen-Bauer I, Haugen JE and Skaugen TE (2011) Temperature and precipitation development at svalbard 1900–2100. *Advances in Meteorology* **2011**, 1–14. doi: 10.1155/2011/893790

Francelino MR and 11 others (2021) WMO evaluation of two extreme high temperatures occurring in february 2020 for the Antarctic Peninsula Region. *Bulletin of the American Meteorological Society* **102**(11), E2053–E2061. doi: 10.1175/BAMS-D-21-0040.1

Grabiec M, Puczko D, Budzik T and Gajek G (2011) Snow distribution patterns on Svalbard glaciers derived from radio-echo soundings. *Polish Polar Research* **32**(4), 393–421. doi: 10.2478/v10183-011-0026-4

Greve R (1997) A continuum–mechanical formulation for shallow polythermal ice sheets. *Philosophical Transactions of the Royal Society of London. Series A: Mathematical, Physical and Engineering Sciences* **355**(1726), 921–974. doi: 10.1098/rsta.1997.0050

Greve R and Blatter H (2009) *Dynamics of Ice Sheets and Glaciers*. Advances in Geophysical and Environmental Mechanics and Mathematics, Springer, Berlin, Heidelberg.

Gusmeroli A (2010) *Polythermal glacier dynamics at Storglaciaren, Arctic Sweden, inferred using in situ geophysical techniques*. Ph.D. thesis, Swansea University.

Gusmeroli A, Jansson P, Pettersson R and Murray T (2012) Twenty years of cold surface layer thinning at Storglaciären, sub-Arctic Sweden, 1989-2009. *Journal of Glaciology* **58**(207), 3–10. doi: 10.3189/2012JoG11J018

Harper JT and Bradford JH (2003) Snow stratigraphy over a uniform depositional surface: spatial variability and measurement tools. *Cold Regions Science and Technology* **37**(3), 289–298. doi: 10.1016/S0165-232X(03)00071-5

Jania J, Mochnacki D and Gadek B (1996) The thermal structure of Hansbreen, a tidewater glacier in southern Spitsbergen, Svalbard. *Polar Research* **15**(1), 53–66. doi: 10.1111/j.1751-8369.1996.tb00458.x

Jonsell UY, Navarro FJ, Bañón M, Lapazaran JJ and Otero J (2012) Sensitivity of a distributed temperature-radiation index melt model based on AWS observations and surface energy balance fluxes, Hurd Peninsula glaciers, Livingston Island, Antarctica. *The Cryosphere* **6**(3), 539–552. doi: 10.5194/tc-6-539-2012

Lapazaran JJ, Otero J, Martín-Español A and Navarro FJ (2016) On the errors involved in ice-thickness estimates II: Errors in digital elevation models of ice thickness. *Journal of Glaciology* **62**(236), 1021–1029. doi: 10.1017/jog.2016.94

Laska M, Grabiec M, Ignatiuk D, Uszczyk A and Kuhn M (2019) Importance of snow as component of surface mass balance of Arctic glacier (Hansbreen, southern Spitsbergen). *Polish Polar Research* **40**(4), 311–338.

Macheret YY, Moskalevsky MY and Vasilenko EV (1993) Velocity of radio waves in glaciers as an indicator of their hydrothermal state, structure and regime. *Journal of Glaciology* **39**(132), 373–384. doi: 10.1017/S0022143000016038

Machío F, Rodríguez-Cielos R, Navarro F, Lapazaran J and Otero J (2017) A 14-year dataset of in situ glacier surface velocities for a tidewater and a land-terminating glacier in Livingston Island, Antarctica. *Earth System Science Data* **9**(2), 751–764. doi: 10.5194/essd-9-751-2017

Martín C, Navarro F, Otero J, Cuadrado ML and Corcuera MI (2004) Three-dimensional modelling of the dynamics of Johnsons Glacier, Livingston Island, Antarctica. *Annals of Glaciology* **39**, 1–8. doi: 10.3189/172756404781814537

McGrath D and 6 others (2018) Interannual snow accumulation variability on glaciers derived from repeat, spatially extensive ground-penetrating radar surveys. *The Cryosphere* **12**(11), 3617–3633. doi: 10.5194/tc-12-3617-2018

Medley B and Thomas ER (2019) Increased snowfall over the Antarctic Ice Sheet mitigated twentieth-century sea-level rise. *Nature Climate Change* **9**(1), 34–39. doi: 10.1038/s41558-018-0356-x

Molina C (2014) *Caracterización dinámica del glaciar Hurd combinando observaciones de campo y simulaciones numéricas*. Ph.D. thesis, Universidad Politénica de Madrid, Madrid.

Molina C, Navarro FJ, Calvet J, García-Sellés D and Lapazaran JJ (2007) Hurd Peninsula glaciers, Livingston Island, Antarctica, as indicators of regional warming: Ice-volume changes during the period 1956–2000. *Annals of Glaciology* **46**, 43–49. doi: 10.3189/172756407782871765

Moore JC and 8 others (1999) High-resolution hydrothermal structure of Hansbreen, Spitsbergen, mapped by ground-penetrating radar. *Journal of Glaciology* **45**(151), 524–532. doi: 10.3189/S0022143000001386

Navarro F and Eisen O (2009) Ground-penetrating radar in glaciological applications. In Pellikka P and Rees WG (eds), Remote Sensing of Glaciers: Techniques for Topographic, Spatial and Thematic Mapping. London, UK: Taylor & Francis, pp. 195–229. doi: 10.1201/b10155

Navarro FJ, Macheret YY and Benjumea B (2005) Application of radar and seismic methods for the investigation of temperate glaciers. *Journal of Applied Geophysics* **57**(3), 193–211. doi: 10.1016/j.jappgeo.2004.11.002

Navarro FJ and 6 others (2009) Radioglaciological studies on Hurd Peninsula glaciers, Livingston Island, Antarctica. *Annals of Glaciology* **50**(51), 17–24. doi: 10.3189/172756409789097603

Navarro FJ, Jonsell UY, Corcuera MI and Martín-Español A (2013) Decelerated mass loss of Hurd and Johnsons Glaciers, Livingston Island, Antarctic Peninsula. *Journal of Glaciology* **59**(213), 115–128. doi: 10.3189/2013JoG12J144

Oliva M and 7 others (2017) Recent regional climate cooling on the Antarctic Peninsula and associated impacts on the cryosphere. *Science of the Total Environment* **580**, 210–223. doi: 10.1016/j.scitotenv.2016.12.030

Otero J, Navarro FJ, Martin C, Cuadrado ML and Corcuera MI (2010) A three-dimensional calving model: numerical experiments on Johnsons Glacier, Livingston Island, Antarctica. *Journal of Glaciology* **56**(196), 200–214. doi: 10.3189/002214310791968539

Pettersson R, Jansson P, Huwald H and Blatter H (2007) Spatial pattern and stability of the cold surface layer of Storglaciären, Sweden. *Journal of Glaciology* **53**(180), 99–109. doi: 10.3189/172756507781833974

Rabus BT and Echelmeyer KA (2002) Increase of 10 m ice temperature: climate warming or glacier thinning? *Journal of Glaciology* **48**(161), 279–286. doi: 10.3189/172756502781831430

Rau F and 8 others (2004) Variations of glacier frontal positions on the northern Antarctic Peninsula. *Annals of Glaciology* **39**, 525–530. doi: 10.3189/172756404781814212

Recio-Blitz C, Navarro FJ, Otero J, Lapazaran J and Gonzalez S (2018) Effects of recent cooling in the Antarctic Peninsula on snow density and surface mass balance. *Polish Polar Research* **39**, 457–480. doi: 10.24425/118756

Robin GDQ, Evans S, Bailey JT and Bullard EC (1969) Interpretation of radio echo sounding in polar ice sheets. *Philosophical Transactions of the Royal Society of London. Series A, Mathematical and Physical Sciences* **265**(1166), 437–505. doi: 10.1098/rsta.1969.0063

Rodríguez R and Navarro F (2015) Study of the fronts of Johnsons and Hurd Glaciers (Livingston Island, Antarctica) from 1957 to 2013, with links to shapefiles. *Pangaea*. doi: 10.1594/PANGAEA.845379

Schannwell C and 5 others (2014) An automatic approach to delineate the cold-temperate transition surface with ground-penetrating radar on polythermal glaciers. *Annals of Glaciology* **55**(67), 89–96. doi: 10.3189/2014AoG67A102

Schroeder DM and 9 others (2020) Five decades of radioglaciology. *Annals of Glaciology* **61**(81), 1–13. doi: 10.1017/aog.2020.11

Sold L and 5 others (2013) Methodological approaches to infer end-of-winter snow distribution on alpine glaciers. *Journal of Glaciology* **59**(218), 1047–1059. doi: 10.3189/2013JoG13J015

Sugiyama S and 7 others (2019) Subglacial water pressure and ice-speed variations at Johnsons Glacier, Livingston Island, Antarctic Peninsula. *Journal of Glaciology* **65**(252), 689–699. doi: 10.1017/jog.2019.45

Turner J, Lachlan-Cope T, Colwell S and Marshall GJ (2005) A positive trend in western Antarctic Peninsula precipitation over the last 50 years reflecting regional and Antarctic-wide atmospheric circulation changes. *Annals of Glaciology* **41**, 85–91. doi: 10.3189/172756405781813177

Turner J and 9 others (2016) Absence of 21st century warming on Antarctic Peninsula consistent with natural variability. *Nature* **535**(7612), 411–415. doi: 10.1038/nature18645

Wen J and 5 others (1998) Glaciological studies on the King George Island ice cap, South Shetland Islands, Antarctica. *Annals of Glaciology* **27**, 105–109. doi: 10.3189/1998AoG27-1-105-109

Ximenis L, Calvet J, Garcia D, Casas JM and Sàbat F (2000) Folding in the Johnsons Glacier, Livingston Island, Antarctica. *Geological Society, London, Special Publications* **176**(1), 147–157. doi: 10.1144/GSL.SP.2000.176.01.11

Zemp M and 5 others (2021) WGMS 2021. Global Glacier Change Bulletin No. 4 (2018-2019). 278.